Since January 2020 Elsevier has created a COVID-19 resource centre with free information in English and Mandarin on the novel coronavirus COVID-19. The COVID-19 resource centre is hosted on Elsevier Connect, the company's public news and information website.

Elsevier hereby grants permission to make all its COVID-19-related research that is available on the COVID-19 resource centre - including this research content - immediately available in PubMed Central and other publicly funded repositories, such as the WHO COVID database with rights for unrestricted research re-use and analyses in any form or by any means with acknowledgement of the original source. These permissions are granted for free by Elsevier for as long as the COVID-19 resource centre remains active.

Talanta 240 (2022) 123207

Contents lists available at ScienceDirect

Talanta

journal homepage: www.elsevier.com/locate/talanta

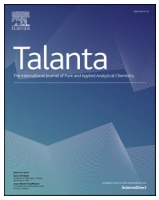

Hybridization chain reaction circuit-based electrochemiluminescent biosensor for SARS-cov-2 RdRp gene assay

Kai Zhang [a,*], Zhenqiang Fan [a], Yue Huang [d], Yuedi Ding [a], Minhao Xie [a], Minghe Wang [b,c,**]

[a] NHC Key Laboratory of Nuclear Medicine, Jiangsu Key Laboratory of Molecular Nuclear Medicine, Jiangsu Institute of Nuclear Medicine, Wuxi, Jiangsu, 214063, China
[b] Department of Colorectal Surgery, Fudan University Shanghai Cancer Center, China
[c] Department of Oncology, Shanghai Medical College, Fudan University, Shanghai, 200032, China
[d] College of Light Industry and Food Engineering, Nanjing Forestry University, Nanjing, Jiangsu, 210037, China

ARTICLE INFO

Keywords:
SARS-CoV-2 RdRp gene
HCR
Y-DNA
Au-g-C_3N_4
ECL

ABSTRACT

In this work, we designed an ECL ratiometric biosensor with a three-stranded Y-type DNA (Y-DNA) probe and induced a hybridization chain reaction (HCR) for the highly sensitive detection of SARS-CoV-2 nucleic acid. The important component of this system is the self-assembled Y-Shaped probe based on three nucleic acids. Y1, Y2, and Y3 can be linked by complementary base pairing to Hairpin1 (H1), Hairpin2 (H2), and Ru modified DNA (Ru1), respectively. H1 and H2 can trigger the HCR reaction when activated by the SARS-CoV-2 RdRp gene and the 5′ end of Ru1. The 5′ end of Ru1 is modified with the Ru complex, which can produce a strong electrochemiluminescence luminescence signal at 620 nm under an applied voltage. Through the amplification of Y-DNA-induced HCR reaction, Ru1 on the electrode surface gradually increased, the ECL signal at 460 nm was gradually quenched, and the signal at 620 nm was steadily generated. The SARS-CoV-2 RdRp gene can be quantified according to the degree of decrease of ECL signal at 460 nm and the increase of ECL signal at 620 nm. Combining the two signal amplification strategies, this ratiometric ECL biosensor can accurately and efficiently detect the target gene with a detection limit of 59 aM.

1. Introduction

Coronavirus Disease 2019 (COVID-19) detection methods mainly contain several nucleic acid detection methods, antibody detection, and antigen detection methods [1]. The current COVID-19 test mainly focuses on antibody and nucleic acid detection. Nucleic acid testing is currently the "standard" for COVID-19 detection, with early diagnosis, high sensitivity, and specificity [2]. However, the antibody test is convenient and rapid and can be used to supplement nucleic acid diagnosis. It is also not suitable for epidemiological investigation in low prevalence areas. Therefore, nucleic acid testing is still an effective tool for rapid and extensive screening of SARS-CoV-2 patients [3]. There are two commonly used nucleic acid diagnostic methods for COVID-19: viral nucleic acid-specific gene testing and viral genome sequencing. The most common method for detecting COVID-19-specific nucleic acid sequences is fluorescent quantitative PCR (polymerase chain reaction) [4,5]. Since COVID-19 is an RNA virus, the kits basically use reverse transcription plus real-time polymerase chain reaction (RT-PCR) to amplify the nucleic acid (RNA) of the pathogen while detecting the amplification products in real-time by fluorescent probes [6].

The PCR system contains a pair of specific primers and a Taqman probe, a particular oligonucleotide sequence labeled with a fluorescent reporter group, and a quenched fluorescent group at each end. If the target sequence is present in the reaction system, the probe binds to the template during the PCR, DNA polymerase degrades the probe enzymatically along the template using the exonuclease activity of the enzyme [7]. The reporter group separates from the quenched group and emits fluorescence. For each DNA strand amplified, a fluorescent molecule is produced. A fluorescent quantitative PCR instrument can monitor the number of cycles in which the fluorescence reaches a predetermined threshold (CT value) is related to the viral nucleic acid concentration; the higher the viral nucleic acid concentration, the smaller the C_T value [8]. However, the method is cumbersome to operate and requires specialized technicians and expensive

* Corresponding author.
** Corresponding author. Department of Colorectal Surgery, Fudan University Shanghai Cancer Center, China.
E-mail addresses: zhangkai@jsinm.org (K. Zhang), wangminghe250@126.com (M. Wang).

https://doi.org/10.1016/j.talanta.2022.123207
Received 17 October 2021; Received in revised form 28 December 2021; Accepted 3 January 2022
Available online 4 January 2022
0039-9140/© 2022 Elsevier B.V. All rights reserved.

experimental instruments. Therefore, the search for novel assays to compensate for the shortcomings of PCR in this area continues.

In recent years, isothermal nucleic acid amplification technology has developed rapidly, and several isothermal amplification methods are highly sensitive, and some have successfully moved to commercialization [9–12]. Depending on the reaction principle, isothermal amplification can be divided into loop-mediated isothermal amplification (LAMP), nucleic acid sequence-based amplification (NASBA), nucleic acid sequence-independent amplification, helicase-dependent amplification (HDA), strand displacement amplification (SDA), and cross-priming amplification (CPA) [7,13–15]. These techniques have advantages and disadvantages and have different applications in nucleic acid detection.

The detection of LAMP amplification products can be done by various methods, including agarose gel electrophoresis, turbidity detection, and color determination [13]. The coloring agents used in the color determination are divided into two categories: one is metal ion indicator, such as calcium xanthophyll, hydroxyl LAMP has the following advantages compared with previous nucleic acid amplification methods: A). The product detection can be judged by visual observation or turbidimeter to detect the turbidity of the precipitate [7]. For RNA amplification, only reverse transcriptase needs to be added to the reaction system, and it can be performed simultaneously (RT-LAMP), no special reagents and instruments are required. B). In most cases, the amplification products can be detected within 20–30 min. The product can be amplified up to 10^9 times, up to 0.5 mg/mL, and quantified in real-time using a special turbidimeter. C). high specificity, because the four specific primers are designed for the six regions of the target sequence, any region in the six regions that do not match the primers cannot be amplified, so its specificity is extremely high. D). high sensitivity, for viral amplification template can reach several copies, which is orders of magnitude higher than PCR. Although LAMP has been widely used in nucleic acid detection and has a tendency to replace PCR, LAMP technology still requires heating and temperature control (65 °C). Therefore, there is still a need to further search for a reaction method that can perform isothermal amplification at room temperature.

On the other hand, electrochemiluminescence (ECL) based sensors have been rapidly developed due to their advantages of low background interference and high sensitivity [1,16,17].ECL sensors have shown potential for ultra-sensitive and real-time analysis. In the ECL process, a substance near the electrode is triggered by an electrochemical method to produce an excited state and generate light emissions. In contrast to photoluminescence, ECL without an excitation source is not affected by autofluorescence background noise and scattered light interference. In addition, the ECL signal is initiated and modulated by the potential with high reproducibility and accuracy. Therefore, ECL sensing shows a reliable sensing process and excellent sensitivity in detection applications.

In this work, we designed an ECL ratiometric biosensor with a three-stranded Y-shaped DNA (Y-DNA) probe and induced a hybridization chain reaction (HCR) for the highly sensitive detection of SARS-CoV-2 nucleic acid. There are three advantages of using a Y-DNA structure. One is that the Y-DNA provides a nucleic acid scaffold for the amplification of nucleic acid on the electrode surface, allowing the HCR amplification product to be firmly anchored on the electrode surface. Second, it induces the HCR reaction, which makes the HCR reaction more efficient. Third, this method does not use the amplification enzyme in the standard amplification system RT-PCR as an essential factor for signal amplification, so it is not necessary to consider false-negative results caused by amplification enzyme inactivation during transportation, storage, and detection. Using this Y-DNA-induced HCR reaction, we achieved detection of SARS-CoV-2 nucleic acid in the pharyngeal swabs with a detection limit of 59 aM.

2. Experimental section

2.1. Chemicals and materials

Gold chloride trihydrate ($HAuCl_4{\cdot}xH_2O$), sodium citrate, and potassium persulfate ($K_2S_2O_8$) were obtained from Aladdin Biochemical Technology Co. Ltd. (Shanghai, China). g-C_3N_4 were obtained from Jiangsu XFNANO Materials Tech, Co. Ltd. (Nanjing, China). Tris (4,4′-dicarboxylic acid-2,2′-bipyridyl) ruthenium (II) dicbloride (Ru(dcbpy)$_3$Cl$_2$) was obtained from Suna Tech Inc. (Suzhou, China). Tris (2-carboxyethyl) phosphine hydrochloride (TCEP) and 6-mercaptohexanol (MCH) were obtained from Sigma-Aldrich (St Louis, MO, USA). The purified DNA sequences (Table S1) were synthesized from Genscript Biotechnology Co. Ltd. (Nanjing, China).

2.2. Preparation of the Au-g-C_3N_4

We successfully synthesized Au-g-C_3N_4 with reference to our previous work [16]. In simple terms, 40 μL of $HAuCl_4{\cdot}xH_2O$ (0.01 M) solution and 4 mL g-C_3N_4 ethanol-water dispersion (15 mg L^{-1}) were mixed and sonicated for 10 min, followed by stirring at room temperature for 4 h to get a mixture solution of g-C_3N_4 and $HAuCl_4$. Then, 30 μL of fresh $NaBH_4$ (0.2 M) solution was injected into the mixed solution and treated in an ice bath condition and retained stirring for 20 min. Continuously, 50 μL of sodium citrate solution was added to the above-mixed solution, and the mixed solution was continuously stirred at 25 °C for 20 min and further continued stirring for another 30 min. Finally, to remove the excess AuNPs, sodium citrate, and $NaBH_4$, the above-mixed solution was washed by ultrapure water and sonicated three times to get the pure Au-g-C_3N_4, which was redispersed in 1 mL of H_2O and stored at 4 °C in a refrigerator for further use.

2.3. Preparation of Y-type DNA

Y-type DNA was prepared by hybridizing three ssDNA, Y1, Y1, and Y3, with concentrations of 4 μM each, mixed in TAE-Mg^{2+} buffer (40 mM Tris buffer, 2 mM EDTA, and 12.5 mM $MgAc_2$). Then, 4 μM of hairpin probes: Hairpin1 (H1), Hairpin2 (H2), and Ru modified DNA (Ru1) were added to the TAE-Mg^{2+} buffer by further incubation at room temperature, resulting in the formation of Ru-DNA complex nanoprobes. Next, the obtained Ru-DNA complex nanoprobes (4 μM) were stored at −20 °C for the following experiments.

2.4. Fabrication of the ratiometric ECL biosensor and target DNA assay

Before starting, the glassy carbon electrode (GCE) was cleaned according to the previous method [18]. 10 μL of Au-g-C_3N_4 was imprisoned on GCE to obtain Au-g-C_3N_4/GCE, and dried at room temperature for about 50 min in the clean air. Subsequently, the prepared Au-g-C_3N_4/GCE was submerged into DNA1 solution containing 10 mM TCEP for 8 h to reduce the S–S bond, thus successfully generating DNA1 modified Au-g-C_3N_4/GCE through Au–S bond formation. Immediately afterward, the above electrode was submerged into 2 mM MCH phosphate (pH 7.4) solution for 40 min at room temperature to passivate the unoccupied sites on the Au particle surface. The sample containing the RdRp gene of a given concentration was mixed with a 100 nM Ru-DNA complex probe in the TAE-Mg^{2+} buffer. The mixture was incubated with DNA1 modified Au-g-C_3N_4/GCE at 37 °C for 3 h to complete the reaction. ECL measurements were carried out at the potential scan of −1.6 - 0 V in phosphate (pH 7.4) solution containing 0.1 M $K_2S_2O_4$. Of note, the biosensor was essential to be cleaned by phosphate (pH 7.4) solution for every step of electrode modification.

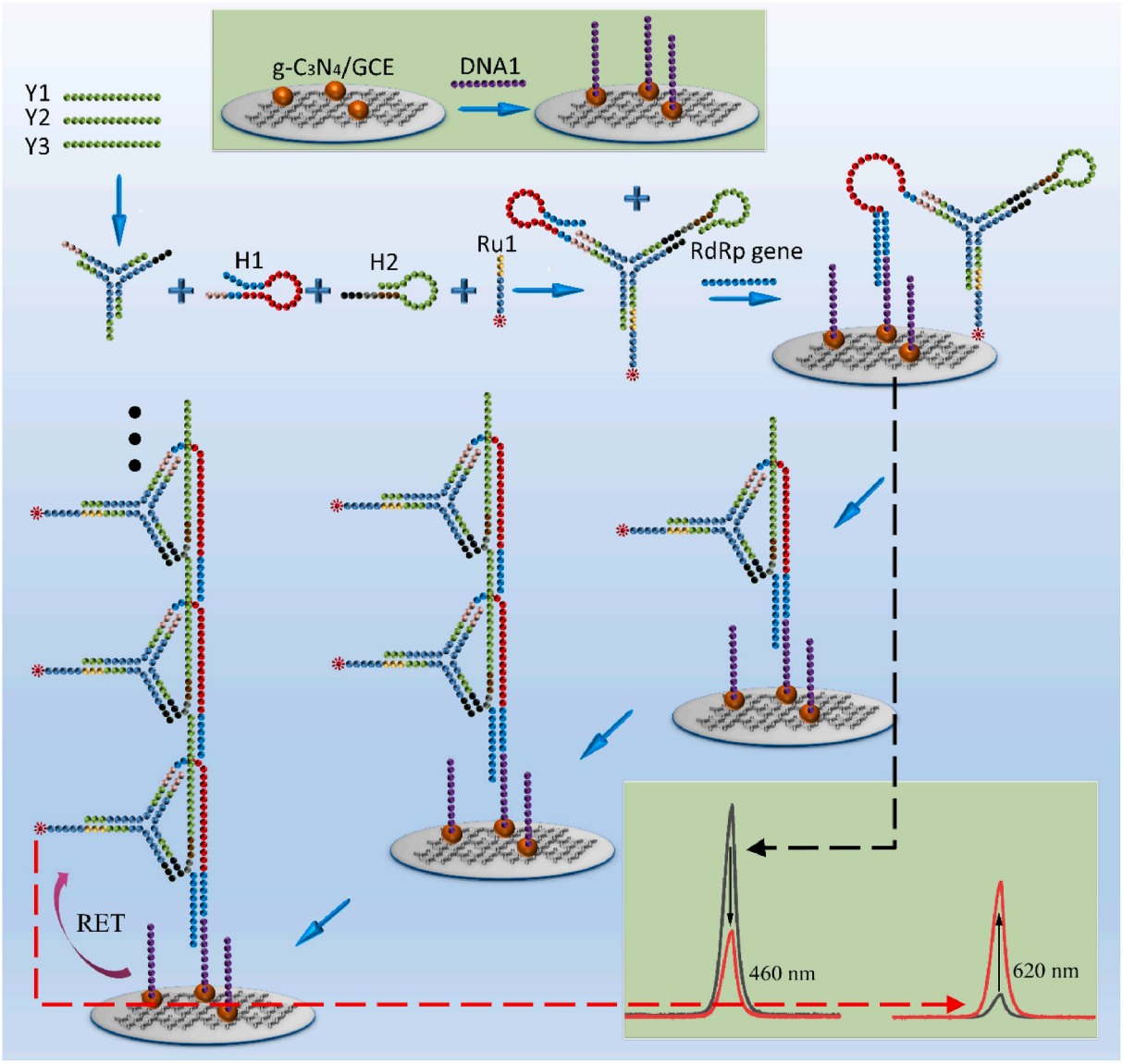

Scheme 1. Schematic illustration of the Y-DNA-induced HCR reaction for the assay of SARS-CoV-2 RdRp gene.

3. Results and discussion

3.1. The working principle of ratiometric ECL biosensor

Based on the amplification strategy of the Y-DNA-induced HCR reaction, we synthesized a ratiometric ECL biosensor to detect the SARS-CoV-2 RdRp gene. The Y-DNA-induced HCR reaction-based amplification strategy principle is shown in Scheme 1. Au-g-C_3N_4/GCE is uniformly modified on the electrode surface, and DNA1 is immobilized on the electrode surface by reacting with Au on the surface of Au-g-C_3N_4/GCE through the –SH group. Another essential component of the system is the Y-Shaped probe, where three DNAs: Y1, Y2, and Y3, can be self-assembled to form a Y-type DNA composite object. Moreover, Y1, Y2, and Y3 can be linked-to H1, H2, and Ru1, respectively, by complementary base pairing. The SARS-CoV-2 RdRp gene activates H1 and H2 to trigger the HCR reaction, and Ru1 is modified with Ru complex at the 5′ end, producing strong electrochemiluminescence at 620 nm with an applied voltage. One part of the SARS-CoV-2 RdRp gene can form a double-stranded DNA1 by complementary pairing with the DNA1 on the electrode surface, and the other part can pair with the H1 in the Y-type probe and open the hairpin structure, and then the activated nucleic acid structural domain in H1 can pair with H2 and open the hairpin and expose the structural trigger domain for the next round of HCR reaction. The activated nucleic acid domain in H1 can then complementarily pair with H2 and open the hairpin to expose the trigger domain for the next round of HCR reaction. Through the amplification of the Y-DNA-induced HCR reaction, Ru1 on the electrode surface gradually increases, and the ECL signal at 460 nm is gradually quenched, and the signal at 620 nm is gradually generated. The SARS-CoV RdRp gene can be quantified according to the degree of reduction of ECL signal at 460 nm and the degree of increase of ECL signal at 620 nm. This ratiometric ECL biosensor can accurately and efficiently detect the SARS-CoV-2 RdRp gene by combining the two signal amplification strategies.

3.2. Possible luminescence mechanism about ECL biosensor

The electrochemiluminescence signal of g-C_3N_4 is obtained when a one-way negative voltage is applied to the system containing the strong oxidant $S_2O_8^{2-}$. Firstly, g-C_3N_4 is reduced to g-$C_3N_4^-$ on the electrode surface, which can generate the intermediate $SO_4\bullet^-$ from $S_2O_8^{2-}$. $SO_4\bullet^-$ is a strong oxidant, and this strong oxidant oxidizes g-$C_3N_4^-$ to g-C_3N_4* excited state. g-C_3N_4* produces the ECL signal when it transitions to the

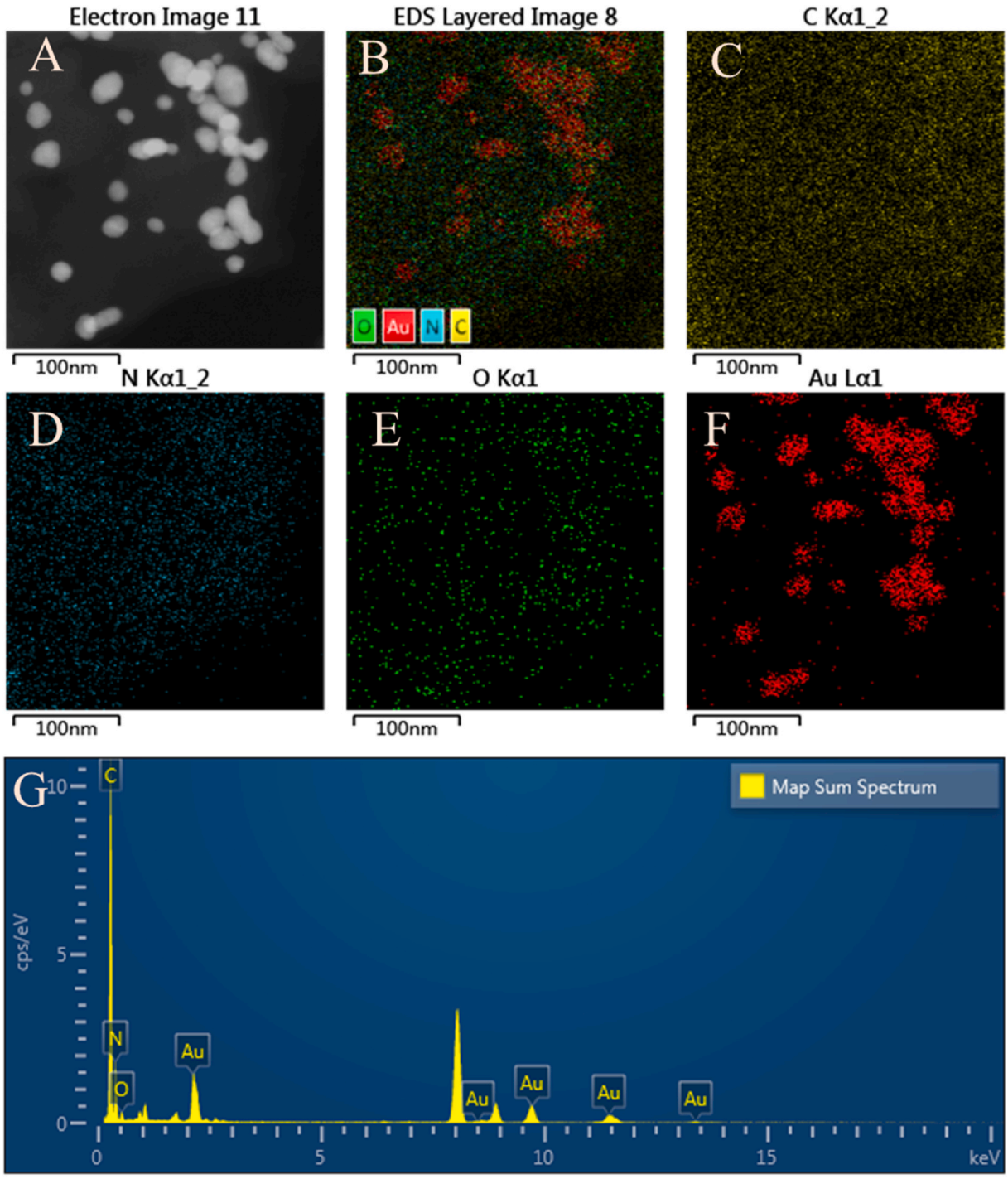

Fig. 1. Elemental mapping data of the Au-g-C_3N_4. (A)–(F) Electron Image, merge image and C, N, O, Au elements, respectively. (G) EDX elemental mapping to show the elemental composites and distribution of the Au-g-C_3N_4.

ground state. The reaction mechanism is as follows.

$$g - C_3N_4 + e^- \rightarrow g - C_3N_4^- \quad (1)$$

$$g - C_3N_4^- + S_2O_8^{2-} \rightarrow g - C_3N_4 + S{\cdot}O_4{\bullet}^- + SO_4^{2-} \quad (2)$$

$$g - C_3N_4^- + SO_4{\bullet}^- \rightarrow g - C_3N_4^* + SO_4^{2-} \quad (3)$$

$$g - C_3N_4^* \rightarrow g - C_3N_4 + hv\ (460\ nm) \quad (4)$$

As previous literature reported [19,20], the UV–Vis spectrum of the g-C_3N_4/Au hybrid has a matching spectral overlap with the ECL emission spectrum of Ru centered at 460 nm, indicating that energy transfer from the g-C_3N_4/Au donor to the Ru acceptor can occur. Therefore, in the construction of the present sensor, only the emission peak of the ECL of g-C_3N_4 (460 nm) needs to be excited, which excites the emission peak of Ru at 620 nm can be obtained using a filter.

3.3. Characterization of Au-g-C_3N_4

Besides, the elemental mapping data (Fig. 1A to Fig. 1F) successfully characterize the elemental distribution of Au-g-C_3N_4. We further performed elemental analysis using energy dispersive X-rays (EDX),

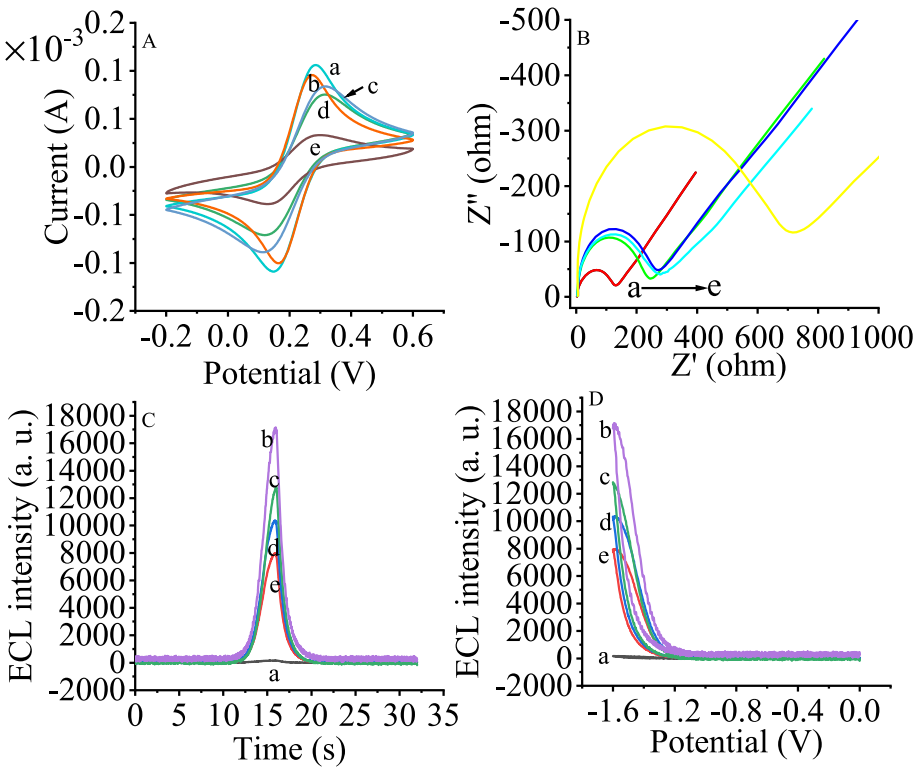

Fig. 2. Characterize the construction of the biosensor by using cyclic voltammetry (A) and EIS (B). Bare GCE electrode (curve a), Au-g-C_3N_4 modified GCE (curve b), GCE modified with Au-g-C_3N_4, DNA1 (curve c), GCE modified with Au-g-C_3N_4, DNA1, and MCH (curve d). GCE modified with Au-g-C_3N_4, DNA1, MCH, the test concentration of RdRp gene (3000 aM), and Ru-DNA complex (curve e). (C) The ECL-Time (D) and the ECL-Potential curves of Bare GCE electrode (curve a), Au-g-C_3N_4 modified GCE (curve b), GCE modified with Au-g-C_3N_4, DNA1 (curve c), GCE modified with Au-g-C_3N_4, DNA1, and MCH (curve d). GCE modified with Au-g-C_3N_4, DNA1, MCH, 1000 aM SARS-CoV-2 RdRp gene, and amplification product (curve e).

depicted in Fig. 1G. The results showed that elemental peaks of C, N, and Au were present in the EDX spectrum of Au-g-C_3N_4. All these elemental characterizations together verify the successful synthesis of Au-g-C_3N_4.

3.4. Characterization of the stepwise fabrication of the ECL biosensor

The cyclic voltammetry (CV) and electrochemical impedance spectroscopy (EIS) plot in Fig. 2A and B depicts the construction process of the biosensor. The impedance value of the naked gold electrode (curve a) is the smallest, indicating that the naked gold electrode has good electrical conductivity. When continuing to modify Au-g-C_3N_4 on the electrode surface and forming a uniform film, the impedance of the modified electrode increases significantly (curve b). When the nucleic acid was modified on the gold nanoparticles, the impedance of the sensor increased significantly (curve c), indicating that the nucleic acid hindered the electron transfer. Subsequently, the assembly of MCH onto the electrode surface similarly increased the impedance value of the sensor (curve d). Finally, the impedance values measured with the test RdRp gene and amplification product modified on the electrode surface are shown in Fig. 2A and B (curve e), and the semicircle of impedance continues to increase. Because the amplification product may further hinder the electron transfer. Therefore, this data indicates the successful assembly of the sensor.

Fig. 2C and D demonstrate the ECL signal intensity during the biosensor construction. The bare GCE showed a very low ECL signal intensity, while the strongest signal was obtained when the GCE was modified by Au-g-C_3N_4 nanocomposite (curve b). Subsequently, DNA1 (curve c) and MCH (curve d) were sequentially modified onto the electrode, corresponding to a successive decrease in ECL signal intensity. When the electrode was incubated with SARS-CoV-2 RdRp gene with amplification product, the ECL signal intensity decreased. These results are consistent with CV and EIS data and successfully demonstrate the synthesis of the biosensor.

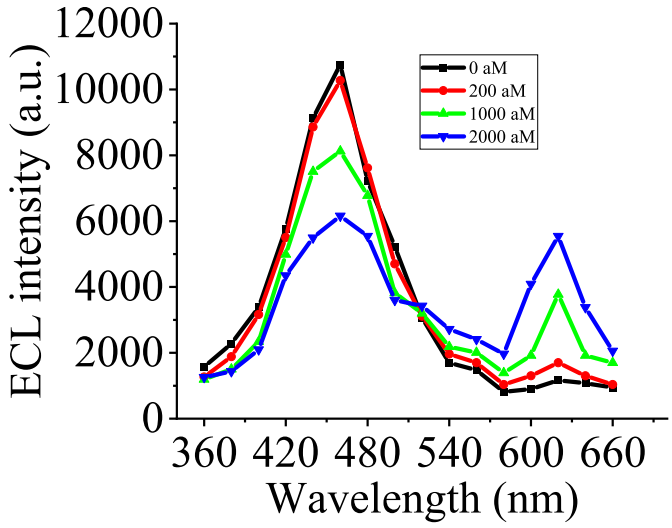

Fig. 3. Ratiometric ECL biosensor at different concentrations (0 aM, 200 aM, 1000 aM, and 2000 aM) of SARS CoV-2 RdRp gene was tested using a series of filters spaced 20 nm apart, measured in 0.1 M PBS (pH = 7.4) containing 0.1 M $S_2O_8^{2-}$.

3.5. ECL-RET mechanism of the ratiometric biosensor

The occurrence of ECL-RET was further verified using filters to collect the maximum spectra. The ECL spectra of SARS CoV-2 RdRp gene at different concentrations were passed through a series of optical filters and were acquired (Fig. 3). When no SARS CoV-2 RdRp gene was present in the detection system, only the emission peak of Au-g-C_3N_4 at 460 nm was detected (black curve). However, as the concentration of SARS CoV-2 RdRp gene increases, the emission peak of Ru at 620 nm continues to increase, which is accompanied by a significant and continuous decrease in the ECL intensity of Au-g-C_3N_4 due to ECL RET (curves b to e). Thus,

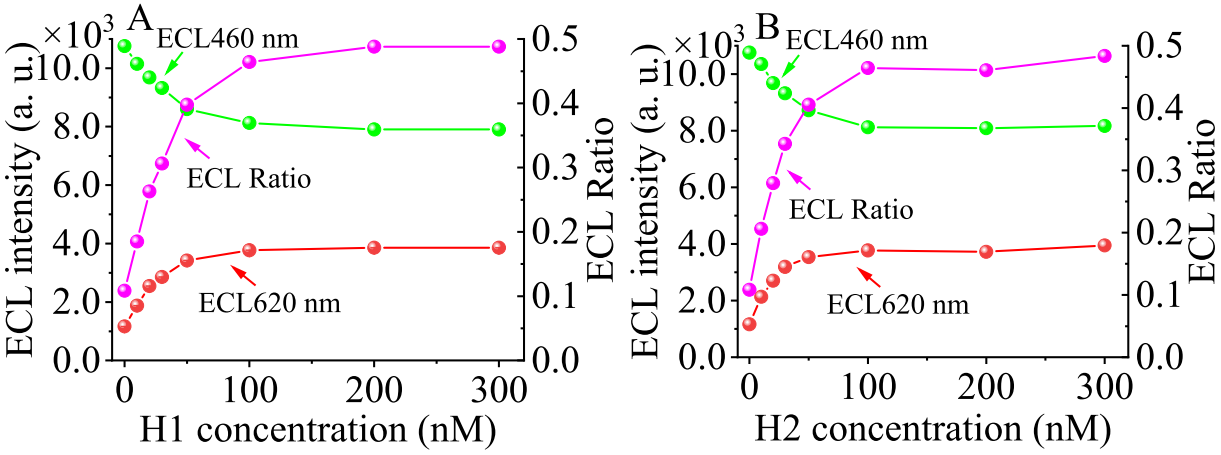

Fig. 4. Optimization of the H1 concentration (A) and H2 concentration (B) for the RdRp gene detection.

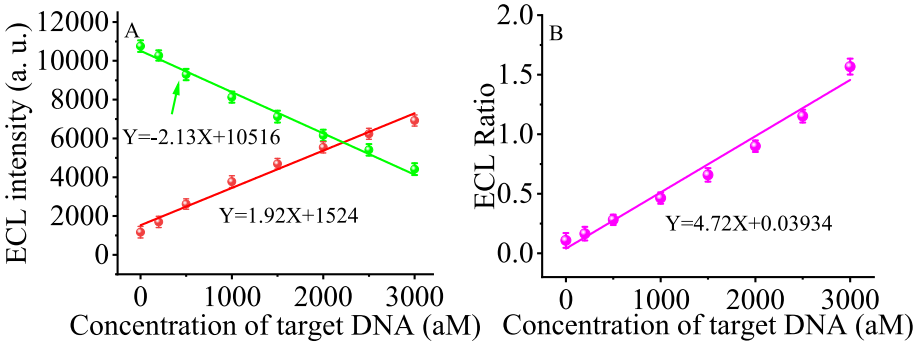

Fig. 5. (A) Relationship between SARS-CoV-2 RdRp gene concentration and ECL intensity of Au-g-C_3N_4 ECL emission at 460 nm (green dots and lines) and Ru ECL emission at 620 nm (red dots and lines). (B) Relationship between SARS-CoV-2 RdRp gene concentration and ECL (ECL_{620}/ECL_{460}). (For interpretation of the references to color in this figure legend, the reader is referred to the Web version of this article.)

this experiment demonstrates the successful construction of the ratiometric biosensor.

3.6. Optimization of analytical conditions

In order to obtain the best performance of the biosensor, some experimental parameters were optimized, including the concentrations of H1, and H2. Fig. 4 shows that the ECL (620 nm) signal intensity gradually increased, and the ECL (460 nm) signal gradually decreased stabilized. Also, the ratio of ECL (620 nm)/ECL (460 nm) increased simultaneously with the increase in H1 and H2 concentrations and reached stability at the concentration of 100 nM for both H1 and H2 concentrations. So, the H1 and H2 concentrations were selected as 100 nM in this study.

3.7. Detection of SARS-CoV-2 RdRp gene in buffer solution

Under the optimized conditions after the previous validation, we used our well-designed ratiometric ECL biosensor to detect the SARS-CoV-2 RdRp gene in the buffer solution. Fig. 5A illustrates the ECL signal changes in the detection system as the concentration of SARS-CoV-2 RdRp increases from 0 aM to 30 fM. The ECL signal intensity gradually decreases at 460 nm and gradually increases at 620 nm. Fig. 5A also depicts the change in ECL signal intensity at 460 nm and an excellent linear relationship between the ECL signal value and the concentration of the SARS-CoV-2 RdRp gene: $y = -2.13X+10{,}516$ ($R^2 = 0.9879$). The change in ECL signal intensity at 620 nm and the concentration of SARS-CoV-2 RdRp gene concentration also showed a good linear relationship: $Y = 1.92X+1524$, ($R^2 = 0.9755$). To make the obtained experimental results more reliable, we further evaluated the change in ECL (620 nm)/ECL (460 nm) values with increasing SARS-CoV-2 RdRp gene concentration: $Y = 4.72 \times 10^{-4} X+0.03934$ ($R^2 = 0.9730$), as shown in Fig. 5B. Based on the limit of detection (LOD) =

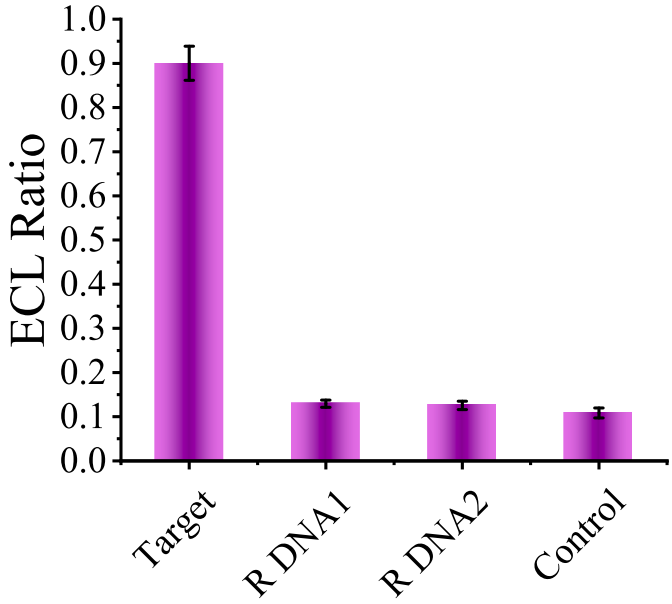

Fig. 6. Selectivity assay by using the biosensor.

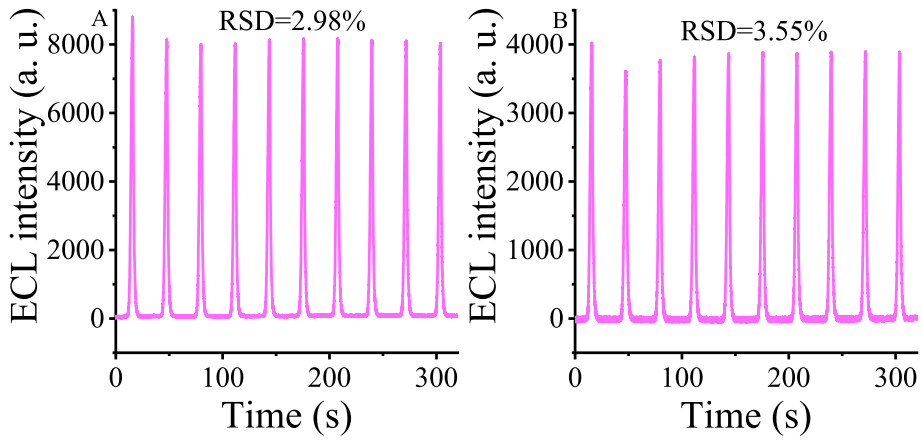

Fig. 7. Stability validation of the biosensor used to detect RdRp gene (A) ECL signal intensity change at 460 nm and (B) ECL signal change at 620 nm. All spectral intensities were repeatedly scanned 10 times after the biosensor detected 1 fM SARS-CoV-2 RdRp gene.

Table 1
Recovery results for the assay of SARS-CoV-2 RdRp in human pharyngeal swabs.

Sample number	Added (aM)	Found (aM)	Recovery (%)	RSD (%, n = 3)
1	50	49.39	98.78	3.84
2	80	79.63	99.54	4.67
3	100	98.35	98.35	3.24
4	200	201.35	100.68	2.56
5	500	505.67	101.13	4.35
6	1000	1012.37	101.24	3.98

3σ/k, the value of LOD was calculated as 59 aM. Our method has a lower detection limit than other methods, as shown in Table S2. The low limit of detection may be due to the fact that we used HCR circuit signal amplification as well as the ratiometric method to process the data.

3.8. Selectivity and stability of the ratio biosensor

To further investigate the selectivity of the ratiometric biosensor, we designed a comparative experiment: some nucleic acids with similar sequences were introduced for control experiments. The ratio sensors prepared under the same experimental conditions were incubated with different targets: 1 fM of SARS-CoV-2 RdRp (Target), 100 fM of Random DNA1 (R DNA1), 100 fM of random DNA2 (R DNA2), and blank samples (Control). As shown in Fig. 6, the ratiometric biosensor incubated with the SARS-CoV-2 RdRp gene exhibited a stronger ECL-RET than the biosensor incubated with other nucleic acid analogs. Thus, the constructed ratiometric biosensor had excellent selectivity. The results indicate that this ratiometric electrochemiluminescent biosensor has good selectivity.

Further to evaluate the stability of the ratiometric biosensor, the modified electrode was incubated with 1 fM SARS-CoV-2 RdRp and subjected to the HCR amplification reaction, and the electrode was scanned continuously for 10 cycles after 320 s of reaction. As seen in Fig. 7, the ECL signal maintained high stability at 460 nm (Figs. 7A) and 620 nm (Fig. 7B) with the relative standard deviation (RSD) of 2.98% and 3.55% when treated with 1 fM SARS-CoV-2 RdRp gene, respectively. The results indicate that the ratiometric biosensor has high stability.

3.9. Detection of SARS-CoV-2 RdRp gene samples in the pharyngeal swabs

To further investigate the resistance of the biosensor for SARS-CoV-2 RdRp gene detection to complex environments, we applied the biosensor to detect the SARS-CoV-2 RdRp gene in normal human pharyngeal swabs. First, we added different doses of the SARS-CoV-2 RdRp gene to pharyngeal swabs by the incorporation method, and then the prepared pharyngeal swab samples were used instead of the standard samples and acted on the biosensor. The biosensor was used to detect the concentration of the SARS-CoV-2 RdRp gene in different pharyngeal swab samples to obtain the signal ratio values corresponding to different concentrations of the SARS-CoV-2 RdRp gene, and the concentration of the SARS-CoV-2 RdRp gene was further calculated based on the ratio values. The recovery results of SARS-CoV-2 RdRp gene detection in normal human pharyngeal swabs are shown in Table 1 as shown in Table 1, the recoveries were all in the range of 98.35%–101.24%, and this result indicates that our designed biosensor can be applied to detect SARS-CoV-2 RdRp gene in human pharyngeal swabs. Therefore, this detection strategy we propose has the potential to be widely used in clinical applications and for the detection of COVID-19-related nucleic acid markers in complex biological samples.

4. Conclusions

In conclusion, we designed an amplification system based on Y-DNA-induced HCR reaction and without amplification enzymes to detect SARS-CoV-2 gene in the pharyngeal swabs. We achieved highly sensitive detection of the SARS-CoV-2 RdRp gene using this method. In this method, we designed a ratiometric ECL-based biosensor to detect the SARS-CoV-2 RdRp gene based on the ECL-RET principle between Au-g-C_3N_4 and Ru. The ratiometric method makes the calculation of the detection limit more accurate and reliable. Since the method does not use the amplification enzyme in the RT-PCR system as an essential factor for signal amplification, it is unnecessary to consider the false-negative results caused by the inactivation of the amplification enzyme during the transportation storage, and detection process. We believe that this method will be more favorable for large-scale screening of COVID-19 in remote areas.

Author statement

Kai Zhang: Conceptualization, Writing, Software. **Zhenqiang Fan**: Data curation, Characterization, Software. **Yue Huang**: Software, Article Modification. **Yuedi Ding**: Data curation, Characterization, Software. **Minhao Xie**: Reviewing, Conceptualization. **Minghe Wang**: Conceptualization

Declaration of competing interest

The authors declare no competing financial interest.

Acknowledgment

This work was supported by the National Natural Science Foundation of China (21705061), and the Jiangsu Provincial Key Medical Discipline (Laboratory) (ZDXKA2016017).

Appendix A. Supplementary data

Supplementary data to this article can be found online at https://doi.org/10.1016/j.talanta.2022.123207.

References

[1] B. Yao, J. Zhang, Z. Fan, Y. Ding, B. Zhou, R. Yang, J. Zhao, K. Zhang, Rational engineering of the DNA walker amplification strategy by using a Au@Ti3C2@PEI-Ru(dcbpy)32+ nanocomposite biosensor for detection of the SARS-CoV-2 RdRp gene, ACS Appl. Mater. Interfaces 13 (17) (2021) 19816–19824, https://doi.org/10.1021/acsami.1c04453.

[2] Z. Fan, B. Yao, Y. Ding, J. Zhao, M. Xie, K. Zhang, Entropy-driven amplified electrochemiluminescence biosensor for RdRp gene of SARS-CoV-2 detection with self-assembled DNA tetrahedron scaffolds, Biosens. Bioelectron. 178 (2021), 113015, https://doi.org/10.1016/j.bios.2021.113015.

[3] G. Qiu, Z. Gai, Y. Tao, J. Schmitt, G.A. KullakUblick, J. Wang, Dual-functional plasmonic photothermal biosensors for highly accurate severe acute respiratory syndrome coronavirus 2 detection, ACS Nano 14 (5) (2020) 5268–5277, https://doi.org/10.1021/acsnano.0c02439.

[4] P. Moitra, M. Alafeef, K. Dighe, M.B. Frieman, D. Pan, Selective naked-eye detection of SARS-CoV-2 mediated by N gene targeted antisense oligonucleotide capped plasmonic nanoparticles, ACS Nano 14 (6) (2020) 7617–7627, https://doi.org/10.1021/acsnano.0c03822.

[5] B. Pang, J. Xu, Y. Liu, H. Peng, W. Feng, Y. Cao, J. Wu, H. Xiao, K. Pabbaraju, G. Tipples, M.A. Joyce, H.A. Saffran, D.L. Tyrrell, H. Zhang, X.C. Le, Isothermal amplification and ambient visualization in a single tube for the detection of SARS-CoV-2 using loop-mediated amplification and CRISPR technology, Anal. Chem. 92 (24) (2020) 16204–16212, https://doi.org/10.1021/acs.analchem.0c04047.

[6] B. Tian, F. Gao, J. Fock, M. Dufva, M.F. Hansen, Homogeneous circle-to-circle amplification for real-time optomagnetic detection of SARS-CoV-2 RdRp coding sequence, Biosens. Bioelectron. 165 (2020), 112356, https://doi.org/10.1016/j.bios.2020.112356.

[7] V.L. Dao Thi, K. Herbst, K. Boerner, M. Meurer, L.P. Kremer, D. Kirrmaier, A. Freistaedter, D. Papagiannidis, C. Galmozzi, M.L. Stanifer, S. Boulant, S. Klein, P. Chlanda, D. Khalid, I. Barreto Miranda, P. Schnitzler, H.-G. Kräusslich, M. Knop, S. Anders, A colorimetric RT-LAMP assay and LAMP-sequencing for detecting SARS-CoV-2 RNA in clinical samples, Sci. Transl. Med. 12 (556) (2020), eabc7075, https://doi.org/10.1126/scitranslmed.abc7075.

[8] V.M. Corman, O. Landt, M. Kaiser, R. Molenkamp, A. Meijer, D.K. Chu, T. Bleicker, S. Brunink, J. Schneider, M.L. Schmidt, D.G. Mulders, B.L. Haagmans, B. van der Veer, S. van den Brink, L. Wijsman, G. Goderski, J.L. Romette, J. Ellis, M. Zambon, M. Peiris, H. Goossens, C. Reusken, M.P. Koopmans, C. Drosten, Detection of 2019 novel coronavirus (2019-nCoV) by real-time RT-PCR, Euro Surveill. 25 (3) (2020) 23, https://doi.org/10.2807/1560-7917.ES.2020.25.3.2000045.

[9] R. Zhou, Y. Li, T. Dong, Y. Tang, F. Li, A sequence-specific plasmonic loop-mediated isothermal amplification assay with orthogonal color readouts enabled by CRISPR Cas12a, Chem. Commun. 56 (24) (2020) 3536–3538, https://doi.org/10.1039/d0cc00397b.

[10] Z. Qing, J. Hu, J. Xu, Z. Zou, Y. Lei, T. Qing, R. Yang, An intramolecular catalytic hairpin assembly on a DNA tetrahedron for mRNA imaging in living cells: improving reaction kinetics and signal stability, Chem. Sci. 11 (7) (2020) 1985–1990, https://doi.org/10.1039/C9SC04916A.

[11] F. Yin, R. Cai, S. Gui, Y. Zhang, X. Wang, N. Zhou, A portable and quantitative detection of microRNA-21 based on cascade enzymatic reactions with dual signal outputs, Talanta 235 (2021), 122802, https://doi.org/10.1016/j.talanta.2021.122802.

[12] J. Deng, J. Xu, M. Ouyang, Z. Zou, Y. Lei, J. Li, Z. Qing, R. Yang, Target-triggered hairpin-free chain-branching growth of DNA dendrimers for contrast-enhanced imaging in living cells by avoiding signal dispersion, Chin. Chem. Lett. (2021), https://doi.org/10.1016/j.cclet.2021.08.046.

[13] M. Zhang, H. Wang, H. Wang, F. Wang, Z. Li, CRISPR/Cas12a-Assisted ligation-initiated loop-mediated isothermal amplification (CAL-LAMP) for highly specific detection of microRNAs, Anal. Chem. 93 (22) (2021) 7942–7948, https://doi.org/10.1021/acs.analchem.1c00686.

[14] F. Iacovelli, A. Idili, A. Benincasa, D. Mariottini, A. Ottaviani, M. Falconi, F. Ricci, A. Desideri, Simulative and experimental characterization of a pH-dependent clamp-like DNA triple-helix nanoswitch, J. Am. Chem. Soc. 139 (15) (2017) 5321–5329, https://doi.org/10.1021/jacs.6b11470.

[15] D. Ossola, M.-Y. Amarouch, P. Behr, J. Voeroes, H. Abriel, T. Zambelli, Force-controlled patch clamp of beating cardiac cells, Nano Lett. 15 (3) (2015) 1743–1750, https://doi.org/10.1021/nl504438z.

[16] Z. Fan, Z. Lin, Z. Wang, J. Wang, M. Xie, J. Zhao, K. Zhang, W. Huang, Dual-wavelength electrochemiluminescence ratiometric biosensor for NF-κB p50 detection with dimethylthiodiaminoterephthalate fluorophore and self-assembled DNA tetrahedron nanostructures probe, ACS Appl. Mater. Interfaces 12 (10) (2020) 11409–11418, https://doi.org/10.1021/acsami.0c01243.

[17] K. Zhang, Z. Fan, B. Yao, T. Zhang, Y. Ding, S. Zhu, M. Xie, Entropy-driven electrochemiluminescence ultra-sensitive detection strategy of NF-κB p50 as the regulator of cytokine storm, Biosens. Bioelectron. 176 (2021), 112942, https://doi.org/10.1016/j.bios.2020.112942.

[18] Y. Wu, X. Li, X. Tan, D. Feng, J. Yan, H. Zhang, X. Chen, Z. Huang, H. Han, A cyclic catalysis enhanced electrochemiluminescence aptasensor based 3D graphene/photocatalysts Cu2O-MWCNTs, Electrochim. Acta 282 (2018) 672–679, https://doi.org/10.1016/j.electacta.2018.06.104.

[19] K. Zhang, Z. Fan, Y. Ding, M. Xie, A pH-engineering regenerative DNA tetrahedron ECL biosensor for the assay of SARS-CoV-2 RdRp gene based on CRISPR/Cas12a trans-activity, Chem. Eng. J. 429 (2022), 132472, https://doi.org/10.1016/j.cej.2021.132472.

[20] J. Ye, L. Zhu, M. Yan, Q. Zhu, Q. Lu, J. Huang, H. Cui, X. Yang, Dual-wavelength ratiometric electrochemiluminescence immunosensor for cardiac troponin I detection, Anal. Chem. 91 (2) (2019) 1524–1531, https://doi.org/10.1021/acs.analchem.8b04640.